REPORT DOCUMENTATION PAGE

Form Approved
OMB No. 0704-0188

1. AGENCY USE ONLY (Leave blank)	2. REPORT DATE	3. REPORT TYPE AND DATES COVERED
	24 June, 1996	Technical 6/1/95 - 5/31/96

4. TITLE AND SUBTITLE
Scanning Probe Lithography. 4. Effect of Scanning Tunneling Microscope Tip Parameters on Lithographic Patterns in Self-Assembling Monolayers

5. FUNDING NUMBERS
N00014-93-1-1338
300x084yip
96PR0-1027

6. AUTHOR(S)
J. K. Schoer and R. M. Crooks

7. PERFORMING ORGANIZATION NAME(S) AND ADDRESS(ES)
Department of Chemistry
Texas A&M University
College Station, Texas 77843-3255

8. PERFORMING ORGANIZATION REPORT NUMBER
20

9. SPONSORING/MONITORING AGENCY NAME(S) AND ADDRESS(ES)
Office of Naval Research
800 North Quincy Street
Arlington, Virginia 22217-5000

11. SUPPLEMENTARY NOTES
Langmuir, submitted.

12a. DISTRIBUTION/AVAILABILITY STATEMENT
Reproduction in whole, or in part, is permitted for any purpose of the United States Government. This document has been approved for public release and sale; it's distribution is unlimited.

12b. DISTRIBUTION CODE

13. ABSTRACT *(Maximum 200 words)*

Here we examine the effect of an STM tip on a Au-confined *n*-octadecyl mercaptan, $HS(CH_2)_{17}CH_3$, SAM in air. We have determined that STM-induced lithography is controlled by a complex combination of parameters defined by both the instrument and the chemical and physical properties of materials in the vicinity of the tip. We have identified conditions that permit accurate control of the tip position during patterning, so we are able to prevent large tip excursions that lead to mixed patterning mechanisms. We propose a multi-step model in which the *n*-octadecyl mercaptan monolayer is: (1) disrupted by the tip, (2) electrochemically desorbed, and (3) removed by the scanning action of the tip. Once the passivating SAM is removed, additional patterning etches the exposed Au substrate. In addition to the primary pattern, we observe an irregularly shaped region of the surface that is disordered for 1 - >500 nm beyond the primary pattern. This disordered region represents an early stage of the patterning and indicates that the resolution of this technique is limited by the electrochemical nature of the patterning process. In some cases it is possible to form secondary patterns from protrusions on the tip. Patterns on *n*-octadecyl mercaptan coated-Au(111) defined in this manner are dimensionally stable for several days. The results provide further insight into this alternative approach to conventional lithography.

14. SUBJECT TERMS	15. NUMBER OF PAGES
	54
	16. PRICE CODE

17. SECURITY CLASSIFICATION OF REPORT	18. SECURITY CLASSIFICATION OF THIS PAGE	19. SECURITY CLASSIFICATION OF ABSTRACT	20. LIMITATION OF ABSTRACT
Unclassified	Unclassified	Unclassified	

[Prepared for publication as an Article in *Langmuir*]

Scanning Probe Lithography. 4. Patterning of *n*-Alkanethiol Self-Assembled Monolayers by Scanning Tunneling Microscopy: Mechanistic Aspects I.

Jonathan K. Schoer and Richard M. Crooks*,[1]

Department of Chemistry

Texas A & M University

College Station, TX 77845-3255

[1]E-Mail: Crooks@chemvx.tamu.edu

Voice: 409-845-5629

Fax: 409-845-1399

*Author to whom correspondence should be addressed

Submitted: April 09, 1996

Abstract

Self-assembled monolayers (SAMs) of *n*-alkanethiol molecules adsorbed onto Au(111) substrates act as lithographic resists which can be selectively patterned using scanning tunneling microscopy (STM). Here we examine the effect of an STM tip on a Au-confined *n*-octadecyl mercaptan, $HS(CH_2)_{17}CH_3$, SAM in air. We have determined that STM-induced lithography is controlled by a complex combination of parameters defined by both the instrument and the chemical and physical properties of materials in the vicinity of the tip. We have identified conditions that permit accurate control of the tip position during patterning, so we are able to prevent large tip excursions that lead to mixed patterning mechanisms. We propose a multi-step model in which the *n*-octadecyl mercaptan monolayer is: (1) disrupted by the tip, (2) electrochemically desorbed, and (3) removed by the scanning action of the tip. Once the passivating SAM is removed, additional patterning etches the exposed Au substrate. In addition to the primary pattern, we observe an irregularly shaped region of the surface that is disordered for 1 - >500 nm beyond the primary pattern. This disordered region represents an early stage of the patterning and indicates that the resolution of this technique is limited by the electrochemical nature of the patterning process. In some cases it is possible to form secondary patterns from protrusions on the tip. Patterns on *n*-octadecyl mercaptan coated-Au(111) defined in this manner are dimensionally stable for several days. Debris from the patterning is located on the tip and in mounds and ridges near the pattern. Our data also indicate

that the tip penetrates the monolayer and very slowly modifies it regardless of bias and tunneling current. The results provide further insight into this alternative approach to conventional lithography.

Introduction

Here, we provide a detailed model for scanning tunneling microscope (STM)-induced removal of *n*-alkanethiol self-assembled monolayers (SAMs) from Au surfaces. The model is based on our prior observation that high tip bias (> ~2.30 V) results in removal of SAMs by Faradaic electrochemical processes.[1] We have previously shown that it is possible to prepare patterns that have critical dimensions of <10 nm,[1,2] and that such patterns can serve as ultramicroelectrodes[3] and platforms for selective chemical vapor deposition (CVD).[4] The motivation for the present study is to better understand the factors that affect the reproducibility of patterning, which should lead to smaller and better resolved patterns.

Most practical lithographic processes rely on visible- or UV-light-induced chemical transformations of organic polymers for fabrication of micron-scale surface features. Critical dimensions of most devices fabricated using present state-of-the-art commercial photolithographic processes are about 0.35 μm,[5-7] although devices having 0.25 μm features are beginning to appear.[8,9] Fabrication of significantly smaller features will require new resists and exposure sources.

Because of the challenges facing existing lithographic methods, we feel it is desirable to evaluate alternative approaches for fabricating structures with critical dimensions in the range 5-200 nm. Although it is unlikely that serial lithographic approaches, such as the one described here, will find large-scale applications, it is reasonable to expect they will be

useful for preparing one-of-a-kind devices and for better understanding the types of materials and process strategies that will be required for the next generation of nanometer-scale devices.

Feature size reduction will necessitate a reduction in resist thickness.[9] Organomercaptan SAMs adsorb onto some metal[10-16] and semiconductor[17-20] substrates to form ultrahigh density lithographic resists approximately 2.5 nm thick. This is thick enough to passivate the Au surface to mass transfer and Faradaic processes,[12,21-34] but it is thin enough to permit electron tunneling or field emission. Organomercaptan SAMs have previously been patterned by micro-contact printing,[35-40] pen writing,[36,41-43] physical abrasion,[36,42-47] electron-[17,48] and ion-beam,[49] methods, photo-oxidation,[50-56] irradiation,[57-60] and scanning probe microscopy (SPM)-based methods.[1,3,4,61-66] Our approach to this problem involves the use of STM to reproducibly and selectively fabricate nanometer-scale patterns in *n*-alkanethiol SAMs.

Numerous mechanisms have been proposed for STM-induced surface modification, including those based on electric fields, current, physical effects such as abrasion, as well as chemical and electrochemical processes.[67-72] STM-induced patterning of *n*-alkanethiol SAMs has generally been accomplished by mechanical abrasion[63,64] or application of a high gap bias.[1,3,4,62,63] The specific mechanism active during STM-induced surface modification is dependent upon the experimental conditions employed. Identification of a specific mechanism (or mechanisms) is a difficult analytical problem for three reasons. First, the size

scale of the patterning precludes far-field optical microscopic or spectroscopic analysis. Second, it is difficult to vary individual experimental parameters while holding all others constant. For example, it is impossible to decouple the tunneling current, gap bias, and tip-sample separation. Third, sequential or multiple simultaneous lithographic mechanisms may be responsible for patterning.

Recently, we identified two distinct bias thresholds relevant to STM-induced patterning of *n*-alkanethiol SAMs confined to Au(111) surfaces.[1,2] At biases between the two thresholds, we are able to consistently and reproducible create patterns less than 10 nm in diameter. We also discovered that a relative humidity exceeding 25% is essential to the patterning process, and partly on the basis of this realization we proposed that the primary patterning mechanism was electrochemical in nature.[1] In experiments conducted at high-humidity (>~70% relative humidity), complete pattern formation readily occurs at biases above ~+2.3 V because a thin layer of water adsorbed to the tip and surface establishes an ultrathin-layer electrochemical cell. The low-energy SAM serves several functions that improve pattern resolution. First, it restricts the dimensions of the highly resistive solution in the tip-substrate gap and confines the patterning to the immediate vicinity of the tip. Second, it passivates unetched regions of the Au(111) substrate. Third, it retards the surface mobility of Au atoms thereby stabilizing the patterns. At low humidity (<~25% relative humidity) there is insufficient water on the SAM surface to support Faradaic

electrochemistry and we do not observe patterning even at biases as high as +5.0 V.

In this paper, we expand upon our previous observations by providing additional information that supports our proposed model. Specifically, we have examined the tip response during patterning, evaluated the impact of several key experimental parameters on patterning, described the physical appearance and dimensions of patterns, identified the location of the lithographic resist after patterning, and studied pattern stability.

Scheme I illustrates the general steps we believe are responsible for the STM-induced patterning of SAM-coated surfaces. The *n*-alkanethiol ($HS(CH_2)_nCH_3$) monolayer is initially well-organized and effectively passivates the surface (Frame 1). In the first patterning step (Frame 2) the STM tip interacts with the SAM causing local disruption of the order within the monolayer even under low bias conditions, which we refer to as standard imaging conditions (SIC, *vide infra*). Although we cannot be certain, it is likely that the tip penetrates the longer chain SAMs ($n \geq \sim 10$).[3,73-78] Tip-induced disorder is likely to be manifest as gauche defects in the methylene chains, movement of sulfur atoms away from the Au three-fold hollow sites, or an untilting of the SAM with a concomitant increase in free volume within the monolayer. All of these effects will reduce the cohesion energy of individual molecules, increase free volume, and destabilize the SAM.[79-81] For example, untilting the SAMs from 30° to 0° with respect to the surface normal will increase the free volume up to ~5%. The additional free volume will facilitate

introduction of gauche defects, penetration of adventitious adsorbates or lithographic debris into the SAM, and finally removal or redistribution of the SAM and substrate (Frame 3a). These processes in turn impede relaxation of the SAM back to its pre-imaged structure and make the monolayer vulnerable to further patterning. It takes several hours of scanning using SIC before these events present themselves as visible changes in images, so the rate at which they occur is slow. As a result, we can reduce the damage to the surface by minimizing the number of times a region is scanned. This part of the model is consistent with several reports indicating that the solvent used during casting, analysis, or modification of a SAM can be incorporated into the monolayer, thereby hindering adsorption of the SAM, or otherwise influence its physical and chemical properties.[10,12,30,31,82-85]

Scheme I

If the events described above are accompanied by a high tip-substrate bias (~+3.0 V), the combination of the locally disrupted monolayer and high bias result in gradual removal of the SAM by Faradaic electrochemical processes (Frame 3b).[1] Removal generates lithographic debris, which consists of SAM fragments and adventitious adsorbates, in the pattern that can subsequently be removed by scanning the tip using SIC; a process we refer to as "sweeping." After sweeping, the SAM is fully, or nearly fully, removed from the surface (Frame 4).

Experimental

Chemicals. *n*-Octadecyl mercaptan (ODM), $HS(CH_2)_{17}CH_3$ (Aldrich, 98%), and 100% ethanol were used as received.

Sample preparation. All substrates were Au balls prepared from ~2 cm lengths of Au wire (0.25 mm diameter, 99.9985% purity, Johnson Matthey) as previously described.[1,3,4,21,34,86-91] We immersed the substrates in ethanolic solutions of ODM (~2.0 mM) for 18-24 h, removed them from solution, rinsed them with absolute ethanol, and dried them under a gentle stream of N_2. This procedure has previously been shown to yield well-ordered, close-packed SAMs that effectively passivate the surface.[3,4,21,34]

STM data acquisition. We used a NanoScope III STM (Digital Instruments, Santa Barbara, CA) for all experiments. Tips were mechanically cut from Pt/Ir wire (80/20%, Ted Pella) and substrates were mounted into a custom holder.[1] The STM *z*-piezo was calibrated by measuring Au(111) monatomic step edges and correlating the mean experimental value to the theoretical Au(111) interlayer spacing of 0.235 nm as previously described.[92] Unless otherwise noted, all images were obtained in air using a D scanner (~12 μm lateral scan range) under ambient humidity conditions, which typically vary between 40% and 70%, and conditions that minimize tip-induced surface damage: ±0.30 V sample bias (positive voltages indicate that the substrate is positive relative to the tip), 150 pA tunneling current, scan rates between 2.0 and 5.0 Hz, and 256 x 256 pixel resolution.[93,94] We refer to these as standard imaging conditions (SIC) in the text. To further minimize tip-

induced surface damage, each region was imaged a minimum number of times, typically ≤ 5 scans.

STM-induced patterning. Except as noted, we patterned the surface using +3.0 V bias, 41 Hz scan rate, 150 pA tunneling current, and 256 x 256 pixel resolution. We refer to these as standard patterning conditions (SPC) in the text. During patterning the desired area was usually scanned 4 times using SPC.

Pattern measurements. To characterize the patterns, we compared images of the surface before, during, and after patterning. We looked for changes in the general appearance of indigenous surface features, depth and lateral dimensions of STM-induced patterns, and RMS roughness of the surface and patterns. Prior to taking measurements, we flattened and planefit each image to eliminate most imaging artifacts. We then used "stop bands" to electronically crop each image to remove any remaining imaging artifacts and Au terraces different from that on which the pattern was formed. The pattern depth we report is the absolute value of the difference between the mean level of the plane of the patterned area and of the adjacent unpatterned terrace. We obtained these values by using the roughness analysis function of the NanoScope software, which calculates the mean level of a selected region by averaging the z values within the selected area relative to the z value of the tip when it first engages the surface.

We used the roughness analysis function of the NanoScope software to calculate the RMS roughness of the patterned and unpatterned regions. The NanoScope software defines the RMS

Roughness (R_q) as $R_q = \{[\sum(Z_i - Z_{ave})^2]/N\}^{1/2}$, where Z_i is the height of individual pixels and Z_{ave} is the average height of the N pixels over which the calculation is performed. To partially account for variability between images and to provide a more useful comparison of changes in the surface roughness, we calculated an RMS roughness factor (RRF) for each image by normalizing the RMS roughness of the target pattern (*vide infra*), or in the case of the unpatterned surface the area to be patterned, to the RMS roughness of the surrounding, unpatterned terrace.[95] The RRF of the unpatterned surface typically ranges from ~0.7 to 1.1 as a result of local variability in the surface roughness.

Results and Discussion

Effect of standard imaging conditions (SIC) on the SAM.

Figure 1a is a 300 nm x 300 nm image of an unpatterned ODM-coated Au surface that is typical of those acquired using SIC. The image is characterized by 2 atomically flat terraces having smooth edges and randomly distributed pits 0.24 nm deep and 2-5 nm in diameter.

Figure 1

The pits are indigenous to organomercaptan-coated Au surfaces and result from a SAM-induced restructuring of the Au surface.[22,65,73,74,96,97] The important point is that these defects are in the Au surface and they are filled with organized organomercaptans and thus do not represent defects in the SAM.

Successive STM images obtained using SIC are virtually indistinguishable from each other for many scans, which indicates that SIC do not rapidly damage the SAM. However, scanning across multiple terraces with high tip velocity or continuously imaging a region for extended periods of time (hours) using SIC does cause visible changes in the surface. In these instances, we have observed combinations of several effects, including smoothing of the Au topography, small ridges at the periphery of the scanned area, eroded terrace edges, slight increases in height (typically <~0.04 nm) in the scanned region, and broadened indigenous pits. However, we have not observed any increase in the depth of the indigenous pits using SIC and there is no change in the measured RMS surface roughness. These results are in general accord with previous observations[64,73] and suggest slow, gradual modification of the SAM, substrate, or both.[98] It is informative to look at these changes more closely and consider their contribution to intentional patterning.

Figure 1b is a 1 μm x 1 μm image obtained after scanning the central 500 nm x 500 nm of the imaged area 4 times using SIC except that the scan rate was a more rapid 41 Hz. We intentionally chose these conditions and this location on the surface to rapidly generate surface changes like those described above. Region A is representative of a region within the scanned area that is slightly elevated (~0.01 nm) when compared with the adjacent terrace.[98,99] We suspect that this observation reveals an early stage of SAM disruption (Scheme I, Frame 3a). Ridges, indicated by arrows B and C, which are probably composed of

mercaptans, mercaptan fragments, adventitious adsorbates, and a small amount of Au, are clearly visible at the edges of this slightly damaged region. Some erosion of the terrace edges and broadening of the indigenous pits within the pattern are also apparent.

Figure 1c is a 329 nm x 329 nm image of the region defined by the dashed line in Figure 1b. This region encompasses the lower-left corner of the area scanned at high tip velocity and also part of the unmodified surface. Ridge B is still clearly visible but is now resolved as a series of islands with x- and y-dimensions of 2-10 nm and up to 30 nm, respectively. By comparing the terrace edges inside and outside the area previously scanned at 41 Hz, we observe erosion of the step edges only inside the previously scanned area. Erosion takes the form of 2-10 nm diameter islands isolated from the adjacent terrace (Feature D) and serrations 2-20 nm in length (Feature E), which result from indigenous pits expanding to become part of the terrace edge. The isolated islands are similar in dimension and shape to the islands that make up ridge B, which may suggest that they are similar in composition.

Consistent with our model, we never observe features like A-E on freshly prepared surfaces, nor do we observe features like D and E outside, nor features like B and C inside, a repetitively scanned area. Clearly these features are the result of disruption, reorganization, and probably partial removal of the SAM, substrate, or both. The data certainly suggest that these

features are not simply the result of tip-induced reorganization of adventitious adsorbates confined to the SAM surface.

Figure 1d was obtained after scanning the region depicted in Figure 1c for more than 3.5 h using SIC. The small islands (Feature D) aggregate into the ridge B and larger islands, suggesting that the composition of the two types of features is similar. Smoothing of terrace edges (Features E and F) and slight broadening of indigenous pits both inside and outside the area scanned with high tip velocity (Features G and H, respectively) are also visible. Since we are able to slightly alter most features, but only eliminate a few, we conclude that the features are not simply physisorbed to the surface and may be bound or intercalated into the SAM (Scheme I, Frame 3a).

Recent reports indicate that heating an *n*-alkanethiol-coated substrate to >350 K anneals the surface by eliminating indigenous pits and, after initially causing serrated step edges, eventually smoothing terrace edges.[73,97,100] The annealing has been attributed to thermally activated diffusion of Au[73] or a mobile Au-mercaptan complex.[100] We may be observing a similar annealing phenomenon here, except that it is induced by the presence of the STM tip. The key point is to recognize that the scanning action of the tip contributes to a very slow rearrangement of the SAM-coated surface, even when using SIC. These types of effects also occur during patterning, and so we conclude that mild mechanical abrasion of the Au/SAM surface by the tip contributes to patterning. Because the modification is slow, we can minimize

changes to the surface by only imaging a particular area a few times.

Large patterns (≥ 500 nm x 500 nm). Figure 2a is an STM image obtained after preparing a nominally 1 μm x 1 μm pattern in an ODM SAM on Au(111) using 4 scans at +8.0 V (scan rate = 2 Hz) followed by 4 sweep scans using SIC (except the scan rate = 2 Hz). The measured x- and y-dimensions of the pattern are 1.00 and 1.05 μm, respectively, and the mean depth of the patterned area is 0.67 nm, indicating that material is removed during patterning. These values are consistent with previous findings for patterns prepared

Figure 2

using these aggressive conditions.[3,4,62] The RMS roughness inside the patterned area is 1.1 nm, while for the region outside the patterned area it is only 0.28 nm. This leads to an RRF^{95} of approximately 4 indicating that the pattern is substantially rougher than the unpatterned surface. A series of step edges (0.26 nm ± 0.02 nm high) are visible in the area outside the patterned region. Two of these, indicated by arrows A and B, extend into the patterned area. This important experiment clearly indicates that even under these harsh conditions surface modification does not drastically alter the underlying Au substrate. As a result, we conclude that the bulk of the patterning is restricted to the SAM, as indicated in Frame 4 of Scheme I.

Location of the patterning debris. Arrows C and D in Figure 2a identify two large ridges outside the pattern and parallel with the slow-scan (y) direction of the STM. We always observe this type of feature in STM images and scanning electron micrographs of large patterns,[3,4,62,93] but only rarely in images of small patterns ($\leq$ 200 nm x 200 nm). We suspect that material removed from small patterns is primarily transferred to the tip (*vide infra*), but when larger patterns are fabricated the tip is unable to accommodate all of this material and the balance is deposited on the surface. Because of their location, dimensions, ability to act as nucleation sites for chemical vapor deposition (CVD),[4] and the increased likelihood of observing them adjacent to large patterns, we believe that the ridges are lithographic debris composed primarily of organomercaptans and organomercaptan fragments that contain a sufficient amount of Au to make them conductive.[4]

Figure 2b is an average depth profile centered on the line through the pattern in Figure 2a.[101] From the dimensions of the pattern, the observed volume of material removed is 7.0×10^5 nm^3. Ridges C and D are clearly visible and average about 1.6 nm and 1.2 nm in height and 120 nm and 140 nm in width (full width at half the maximum height), respectively. On the basis of these dimensions, we estimate that ~3.6×10^5 nm^3 of material is present in the two ridges. Individual mounds are clearly visible within (Feature E) and to the sides (Feature F) of the pattern. We do not observe mounds above or below the pattern, suggesting that the material within the mounds is lithographic debris. The mounds

contain approximately 1.5 x 10^5 nm^3 of material, so together with the ridges we can account for approximately 70% of the material removed from the pattern.

These calculations are clearly an estimate because of uncertainty about the tip position and composition and packing of the material in the ridges and mounds. However, if we assume that the packing density of the ridges and mounds is similar to the unpatterned monolayer (ODM is a solid at room temperature and pressure) and that the tip penetrates into the debris and unpatterned surfaces to the same extent, the estimate is reasonable and accounts for a significant fraction of the debris. Consistent with Scheme I and the results illustrated in Figure 1, repeated scanning across the ridges and mounds using SIC only partially removes them, indicating that they are fairly strongly bound to the SAM.

It has been established that material can be transferred between a substrate and STM tip,[102-104] and Figure 2c provides evidence that some debris from the pattern is transferred to the tip in our experiment. Figure 2c is the first image acquired after fabricating a nominally 50 nm x 50 nm pattern by scanning the surface 4 times at +3.0 V bias, 41 Hz scan rate, 150 pA tunneling current, and 256 x 256 pixel resolution (SPC). The slow-scan direction of the tip was from the top of the image to the bottom. The indigenous pits at the top of the image and most of the STM-induced pattern are well-resolved. However, after the tip has almost reached the bottom of the pattern, the resolution of the image degrades. Similar resolution changes in other images

virtually always occur as the tip is scanning across a pattern, not when scanning unpatterned portions of the surface. We attribute the degradation of image quality to debris from the patterned area transferring from the surface to the tip.[105]

Extended patterning and disorder. We can identify four unique regions on a surface after patterning. These are delineated in Figure 2c. The first region is the unmodified part of the surface. Located outside the white oval, it is characterized by a largely intact, unmodified SAM (the light gray areas to the left and right of the pattern are imaging artifacts that result from the time response of the piezoelectric scanner). The second region is the 50 nm x 50 nm primary pattern where most of the SAM has been removed, which is located inside the solid square. For identifying the patterning mechanism and determining the resolution limits of this method, two other regions are of interest. Between the dashed and solid squares, ~5 nm of patterning that extends beyond the primary pattern is visible. This "extended" patterning results from a combination of microscope drift during patterning[106] and the electrochemical basis of SAM removal.[1] Because we are unable to identify any differences in the properties of the primary and extended patterns, we treat them here as a single "primary" pattern.

The fourth distinct region, which we term the "disordered" region is located between the oval and dashed square. This area is characterized by apparent disordering of the surface for a substantial distance beyond the primary pattern (~30 nm in Figure 2c). It is important to recognize that the tip does not scan this

area during primary pattern formation and therefore this disordering is caused by an indirect interaction between the tip and surface. The size, shape, and position of the disordered region relative to the primary pattern is dependent on both the tip shape and relative humidity. In Figure 2c the disordered region extends somewhat further to the left side of the pattern than to the right. In other cases, we observe little or no disordered region and occasionally we observe disordered regions that extend for hundreds of nanometers. We believe that this disordering represents an initial stage of patterning, such as the partial removal, oxidation, or cleavage of the SAM (Scheme I, Frames 2, 3a, and 3b), which reduces its passivating ability. This is supported by *in situ* electrochemical STM experiments in which we observe that Au in the vicinity of both the primary pattern and disordered region are preferentially etched by CN^- compared to the unmodified surface region.[107] Figure 2d is an average depth profile[101] centered on the line in Figure 2c. At Point G the tip enters the disordered region and the average depth slowly increases as the tip approaches the primary pattern, indicating a gradual decrease in the amount of organomercaptan on the surface. At point H a large change in the slope occurs as the tip enters the primary pattern. These results are consistent with our proposed model, but they imply that the ultimate resolution of this method is limited by the extended patterning and disordering, rather than by the dimensions of individual molecules as we might have hoped.

Small patterns (≤ 200 nm x 200 nm). Figure 3a is an image of an ODM-coated Au(111) surface prior to patterning. The surface is characterized by a small Au island, indicated by an arrow, and a large Au terrace covered with indigenous pits. The step height between the island and terrace is 0.23 ± 0.02 nm, close to the 0.235 nm expected for an atomic Au step.

Figure 3

Figure 3b shows the same region after fabricating a nominally 100 nm x 100 nm pattern using SPC and 4 scans. A dashed box outlining the pre-patterned area is shown in Figure 3a for comparison. The pattern is representative of many we have fabricated using these conditions. There is no change in the unpatterned areas of Figure 3b, but in and near the patterned region we observe extended patterning and an increase in the depth and roughness of the patterned area, just as we observed for the larger patterns. Indigenous pits are clearly visible within the pattern after fabrication, indicating that the patterning is restricted primarily to the SAM. Several pits are highlighted in Figures 3a and 3b. The pits within the pattern have broadened and merged after fabrication, as we observe after repetitively scanning an area with SIC, but more intensive patterning is required before they are obliterated (*vide infra*). In contrast to Figure 2a, there are no large debris ridges or mounds, suggesting that most of the organic material has been transferred to the tip.

Figures 3c-3f are STM images obtained during the 4 scans used to convert the surface from that shown in Figure 3a to that in Figure 3b. Since the image quality is high and the tip-substrate separation is approximately constant throughout patterning, we infer that the *z*-piezo feedback mechanism is able to accurately control the position of the tip. As a result, we believe that the patterning mechanism does not change during patterning with moderate biases ($\geq$ ~+2.3 V and $\leq$ ~+3.5 V). This is in contrast to what we observe when we fabricate patterns at high biases (> ~+3.5 V), e.g. Figure 2a. Images similar to those shown in Figures 3c-3f, but obtained under high bias patterning conditions, indicate the feedback mechanism of the *z*-piezo is unable to accurately control the tip-substrate separation and rapid, frequent, and large changes in tip-substrate separation occur. These changes in tip-substrate separation in turn cause variability in the field strength and current, making it impossible to identify a single patterning mechanism. Consistent with our model of gradual surface patterning, the RMS roughness of the images shown in Figure 3c-3f increase from a value of 0.14 nm in Figure 3c to 0.19 nm in Figure 3f. Additionally, indigenous pits are clearly visible in Figure 3c and, although they become progressively more obscure, several pits remain visible throughout surface modification, indicating that patterning is restricted primarily to the SAM. Two such pits are highlighted in Figures 3c-3f.

Repetitive patterning. Figure 4 and Table I illustrate the impact of repeatedly patterning a nominally 50 x 50 nm pattern into an ODM-coated Au(111) surface using SPC. Figures 4a-4d are

images obtained after 1, 10, 60, and 250 patterning cycles, respectively. The images have been inverted and displayed in three dimensions to emphasize the pattern depth. Clearly, repetitive patterning results in a progressive increase in pattern depth (Feature A). As discussed earlier, the grooves that are apparent on either side of the pattern (Feature B in Figure 4d) are imaging artifacts. The x- and y-dimensions of the primary pattern also increase as the number of patterning scans increases, reaching 60 and 58 nm, respectively, after 250 patterning scans. Indigenous pits within the pattern are easily identified in Figure 4a and even after 10 scans at +3.0 V (Figure 4b) they are apparent.

Figure 4

Table I

Two interesting features are visible on the terrace adjacent to the pattern. First, a disordered region (Feature C) is clearly visible around the primary pattern. Both the lateral dimensions and depth of the disordering increase as the number of patterning cycles increase, just as observed for the primary pattern. These observations are consistent with the disordered region representing an early stage of patterning.

Figure 4b also clearly shows formation of a secondary pattern (Feature D). The secondary pattern is likely the result of a protrusion on the tip that is in close proximity to the surface. Such protrusions are common features on cut tips like those used

here, and they provide additional points where electrochemical patterning can proceed. Both the primary and secondary patterns have similar lateral dimensions, but as shown in Figures 4c and 4d and in Table I, repetitive patterning does not increase the depth of the secondary pattern as rapidly as the primary pattern, nor does the RRF of the secondary pattern increase as dramatically. The presence of the secondary pattern argues strongly against an electron-beam (field emission or tunneling)-based patterning mechanism, since this would require that electrons tunnel simultaneously from two distinct points on the tip. Because electrons tunnel through the lowest barrier, and since we do not observe any multiple images with this tip, essentially all the current flows through the primary tip, not through the second protrusion on the tip and into the secondary pattern.

The presence of a secondary pattern has important implications for the use of arrays of STM tips for micro- and nano-fabrication. Our data illustrate that it is possible to use multiple tips to pattern a surface, however, the data also clearly illustrate the difficulty that small differences in the heights of individual tips in arrays will present.

As shown in Figure 4e, the primary pattern depth remains approximately constant at ~0.32 nm during the first 10-12 patterning scans. Figure 4f shows that during this same time the RRF decreases, indicating that repetitive scanning smoothes the pattern bottom. These results suggest that after initially patterning the SAM, the tip must remove or redistribute sufficient material within the pattern to further expose the surface, which

takes 10-12 scans, before the depth again increases (Scheme I, Frames 3b and 4). The indigenous pits start to become obscure after 10-12 scans also, suggesting that the Au itself begins to be patterned at this point. The RRF, however, continues to decrease until after approximately 40-50 scans (a depth of ~0.60 nm), at which point further scanning begins to roughen the surface. We believe that between scans 10 and 50 there is insufficient material to fully passivate the surface, but there is enough to facilitate tip-induced smoothing of the surface. Once this layer is removed, the Au substrate begins to be roughened more substantially. After 250 patterning scans using SPC the pattern depth reaches ~3.0 nm, a value substantially greater than the thickness of the ODM monolayer (~2.5 nm). From these results, we are confident that the pattern is well into the Au substrate after 250 patterning scans, and that patterning of the Au probably begins at an apparent depth between 0.30 nm and 0.60 nm. If this estimate is correct, it means the tip is deeply embedded within the SAM from the start of the patterning process.

Repetitive "sweeping". Figure 5a shows an inverted image of a nominally 100 nm x 100 nm pattern immediately after patterning with 4 scans using SPC. Indigenous pits are visible inside and outside of the pattern after the lithography. The actual x- and y-dimensions of the pattern are 106 nm and 107 nm, respectively. Immediately after patterning the average depth of the pattern is 0.22 nm and the RRF is 2.0.

We have found that once a pattern is formed, its permeability[3] and resolution can be greatly improved by scanning

within the pattern several times using SIC. We term this second lithographic step "sweeping." Figure 5b shows the same region as in Figure 5a, but after 8 sweep scans using SIC within the

Figure 5

pattern. The unpatterned terrace, which is not scanned by the tip during sweeping, adjacent to the pattern is unchanged. Even after 125 sweep scans we do not observe any secondary patterning, increase in the lateral dimensions of the primary pattern, or extended disorder, which is in contrast to results obtained using SPC (Figure 4). However, consistent with Figure 4 and Frame 4 of Scheme I, the pattern is visibly deeper and smoother, indicating that material is removed from and redistributed within the pattern. Additionally, the indigenous pits inside the pattern broaden slightly and are less well-resolved, suggesting that some of the material removed or redistributed is Au.

Figure 5c shows that the pattern depth increases from 0.22 nm to 0.42 nm after 4 sweep scans. The depth of the pattern then varies with additional sweeping, but generally remains between 0.3 nm and 0.4 nm. This behavior is similar to that observed during the first 10-12 scans shown in Figure 4e and suggests that similar events are occurring during this time frame regardless of whether we are patterning or sweeping the pattern. Importantly, the measured pattern depth does not change after the first few sweeping scans, which indicates that material is permanently

removed from the pattern, but that additional sweeping using SIC does not remove or deposit more material therein.

The pre-lithography RRF of the region of the surface shown in Figures 5a and 5b is 1.0 (Figure 5d). After lithography, the RMS roughness of the surrounding terrace is unchanged, however, the RRF increases to 2.0, indicating that the pattern roughness increases dramatically. Repetitive sweeping of the pattern initially causes the RRF to increase to 2.1 nm after 4 sweep scans, but it then steadily decreases to a value of 1.2 after 125 sweep scans. This behavior is similar to what we observed during the first 50-60 patterning scans in Figure 4f, supporting our claim that material is being rearranged by the tip to smooth the pattern bottom. Unlike repetitive patterning of a surface using SPC, repetitive sweeping of the surface using SIC causes the RRF to eventually approach its pre-patterning value, a clear sign that no further removal of material occurs.

The data shown in Figures 4 and 5 suggest that after lithography, the bottom of the pattern is covered with two types of material. The first type is easily removed during the first several sweep or patterning scans. It probably consists of SAM debris that does not bind strongly to the Au surface, e.g. hydrocarbon fragments, sulfonates, or very small Au clusters that may be covered with organic material. The facile removal of this material is reflected in the initial large increase in the pattern depth, even though the bias conditions are not aggressive, and small increase in the RRF during both repetitive sweeping and patterning experiments. The second type of material is, we

believe, more tightly bound to the surface than the first. Repetitive patterning using SPC redistributes and removes this material, however, repetitive sweeping using SIC only redistributes it. Although the material is tightly bound to the surface, it does not passivate the surface. The key point is that only after the SAM is severely disrupted as a result of using SPC can SIC be used to significantly alter the pattern characteristics.

Pattern stability. The results illustrated by Figures 1, 4, and 5 indicate that the *n*-alkanethiol-coated surface is somewhat mobile under the influence of the tip when using SIC. The question arises of whether the surface mobility occurs only under the influence of the scanning tip or if tip-independent surface diffusion is also operative. As discussed earlier, several groups have shown that heating an organomercaptan-coated substrate to >350 K anneals the surface, eliminating the indigenous pits, and eventually smoothing terrace edges.[73,97,100] Whether a similar annealing phenomenon occurs at lower temperature in the absence of the tip will affect the long-term stability of the pattern and bear on the suitability of this approach for technologically significant lithographic applications.

To evaluate the stability of the pattern and the contribution of the tip to the observed surface mobility, we fabricated a nominally 50 nm x 50 nm pattern with 4 scans using SPC and imaged it on 5 consecutive days. Between images we stopped scanning the tip and parked it ~2 μm away from the pattern center. Figure 6 shows the results of this experiment. Figure 6a shows the pattern

immediately after fabrication. Table II lists some of the physical characteristics of the pattern and how they change as a function of time. Initially the x- and y-dimensions of the primary pattern are 55 nm and 54 nm, respectively, and the pattern is ~0.50 nm deep. A disordered region is clearly visible. Indigenous pits are apparent on the adjacent unpatterned terrace and within the disordered region, however they are not present within the pattern, suggesting that the Au surface has been disturbed. The raised features located to the left and right of the pattern are imaging artifacts.

Figure 6

Table II

Figure 6b shows the same pattern 24 h later. The general appearance of the unpatterned terrace is unchanged. This is confirmed by the data shown in Table II, which indicate that the RMS roughness of the terrace remains essentially constant. The appearance of the primary pattern is also similar to Figure 6a. The depth and RMS roughness of the pattern decrease only slightly even after 95 h (Table II). The lateral dimensions of the primary pattern do not change. Clearly, the primary pattern and undamaged SAM are very stabile in the absence of a scanning tip.

In contrast to the primary pattern, the disordered region changes dramatically. The disorder has apparently segregated into more well-defined regions that present themselves as a series of islands and terrace edges. A number of the indigenous pits within

the disordered region that were clearly visible in Figure 6a are obscured in Figure 6b (solid box in Figures 6a and 6b). We believe these effects result from molecules within and adjacent to the disordered region reorganizing themselves and the Au substrate to maximize the intermolecular forces that strongly stabilize the monolayer. The key point, however, is that the undamaged SAM and primary pattern are both stable in the absence of the scanning tip.

Naked Au. Figure 7a is an inverted STM image obtained prior to patterning a nominally naked Au(111) surface in air. The surface is characterized by a single large terrace, a portion of a lower terrace, and several small islands.[108] The height of the steps is 0.23 ± 0.01 nm, in good agreement with the theoretical value. In contrast to mercaptan-coated surfaces, there are no small indigenous pits on the surface.

Figure 7

Figure 7b shows the same region after lithographically defining a nominally 50 nm x 50 nm pattern with 4 scans using SPC. The surface features are unchanged except for the newly formed pattern.[109] Although patterns prepared on bare Au are generally irregular in shape, this one is approximately square with lateral dimensions of 70 nm x 70 nm, an average depth of ~1.5 nm, an RMS roughness of 0.79 nm, and an RRF of 5.6. Each of these values is substantially greater than we observe after the first several patterning scans of ODM-coated Au, but they are similar to the

values that result after more than 150 patterning scans (Figure 4e and 4f). This strongly implies that the SAM patterning process eventually involves the substrate. These results are in agreement with our previous findings that patterning naked Au is less difficult than ODM-coated Au.[1,2] They are also consistent with prior electrochemical studies, which demonstrated that SAMs prepared from long-chain, *n*-alkanethiols such as ODM are effective at passivating Au surfaces toward Faradaic processes,[12,21-31] including CN^--induced Au etching.[32-34] The key point is that in the absence of the hydrophobic monolayer, pattern resolution, reproducibility, and stability are substantially decreased, which is fully consistent with our electrochemical patterning model.[1] The reasons for this are threefold. First, the low-energy SAM minimizes the thickness of the water layer on the surface, which confines patterning to the immediate vicinity of the tip. Second, the SAM passivates unetched regions of the Au surface, which promotes anisotropic etching. Third, the SAM retards the surface mobility of Au atoms and thereby stabilizes the pattern.

Conclusion

STM-induced lithography of *n*-alkanethiol-coated surfaces is a complex process controlled by a number of parameters. However, we have identified conditions that allow us to reproducibly pattern and subsequently characterize such patterns. The lithography is a multi-step process that is consistent with the model shown in Scheme I: (1) tip-induced disruption of the SAM; (2) electrochemical desorption and additional disruption of the SAM;

and (3) removal of lithographic debris from the resulting pattern by the tip. This is an important factor to consider for designing fabrication schemes suitable for the preparation of nanometer-scale electrodes[3] or other devices. By limiting the applied bias and duration of the lithography, the patterning is restricted to the monolayer and high-resolution patterns that are dimensionally stable for several days result. As illustrated by the difference in the patterns obtained on naked Au and ODM, the impact of changing the gap environment holds particular promise for reproducibly fabricating nanoelectrodes and other lithographic features with high resolution.

Acknowledgments

Full support of this research by the Office of Naval Research is gratefully acknowledged. JKS gratefully acknowledges an IBM Manufacturing Research Fellowship and a Joseph W. Richards Summer Fellowship from the Electrochemical Society. We appreciate insightful discussions with Dr. Omourtag Velev, Dr. Roland Allen, and Dr. Michael Weimer (Texas A & M University).

References

(1) Schoer, J. K.; Zamborini, F. P.; Crooks, R. M. *J. Phys. Chem.* **1996**, submitted.

(2) Schoer, J. K.; Crooks, R. M., manuscript in preparation.

(3) Ross, C. B.; Sun, L.; Crooks, R. M. *Langmuir* **1993**, *9*, 632-636.

(4) Schoer, J. K.; Ross, C. B.; Crooks, R. M.; Corbitt, T. S.; Hampden-Smith, M. J. *Langmuir* **1994**, *10*, 615-618.

(5) Allen, R. D.; Wallraff, G. M.; Hofer, D. C.; Kunz, R. R.; Palmateer, S. C.; Horn, M. W. *Microlith. World* **1995**, *4*, 21-26.

(6) Silverman, P. J. *Microlith. World* **1995**, *4*, 7-8.

(7) Thompson, T. *Byte* **1996**, *21*, 45-54.

(8) Arnold, W. H. *Microlith. World* **1995**, *4*, 7-11.

(9) Sparkes, C.; Thompson, L.; Bischoff, P. *Microlith. World* **1995**, *4*, 14-15.

(10) Ulman, A. *An Introduction to Ultrathin Organic Films: from Langmuir-Blodgett to Self-Assembly*; Academic Press Inc: San Diego, 1991, pp 1-442 and references therein.

(11) Dubois, L. H.; Nuzzo, R. G. *Annu. Rev. Phys. Chem.* **1992**, *43*, 437-463 and references therein.

(12) Bain, C. D.; Troughton, E. B.; Tao, Y.-T.; Evall, J.; Whitesides, G. M.; Nuzzo, R. G. *J. Am. Chem. Soc.* **1989**, *111*, 321-335 and references therein.

(13) Laibinis, P. E.; Whitesides, G. M.; Allara, D. L.; Tao, Y.-T.; Parikh, A. N.; Nuzzo, R. G. *J. Am. Chem. Soc.* **1991**, *113*, 7152-7167.

(14) Laibinis, P. E.; Whitesides, G. M. *J. Am. Chem. Soc.* **1992**, *114*, 1990-1995.

(15) Laibinis, P. E.; Whitesides, G. M. *J. Am. Chem. Soc.* **1992**, *114*, 9022-9028.

(16) Nuzzo, R. G.; Allara, D. L. *J. Am. Chem. Soc.* **1983**, *105*, 4481.

(17) Tiberio, R. C.; Craighead, H. G.; Lercel, M.; Lau, T.; Sheen, C. W.; Allara, D. L. *Appl. Phys. Lett.* **1993**, *62*, 476-478.

(18) Sheen, C. W.; Shi, J.-X.; Martensson, J.; Parikh, A. N.; Allara, D. L. *J. Am. Chem. Soc.* **1992**, *114*, 1514-1515.

(19) Lunt, S. R.; Santangelo, P. G.; Lewis, N. S. *J. Vac. Sci. Technol. B* **1991**, *9*, 2333-2336.

(20) Lunt, S. R.; Ryba, G. N.; Santangelo, P. G.; Lewis, N. S. *J. Appl. Phys.* **1991**, *70*, 7449-7467.

(21) Chailapakul, O.; Crooks, R. M. *Langmuir* **1993**, *9*, 884-888.

(22) Chailapakul, O.; Sun, L.; Xu, C.; Crooks, R. M. *J. Am. Chem. Soc.* **1993**, *115*, 12459-12467.

(23) Finklea, H. O.; Snider, D. A.; Fedyk, J. *Langmuir* **1990**, *6*, 371-376.

(24) Finklea, H. O.; Avery, S.; Lynch, M.; Furtsch, T. *Langmuir* **1987**, *3*, 409-413.

(25) Finklea, H. O.; Snider, D. A.; Fedyk, J. *Langmuir* **1993**, *9*, 3660.

(26) Sabatani, E.; Rubinstein, I.; Maoz, R.; Sagiv, J. *J. Electroanal. Chem.* **1987**, *219*, 365-371.

(27) Sabatani, E. R., Israel *J. Phys. Chem.* **1987**, *91*, 6663-6669.

(28) Miller, C. J.; Cuendet, P.; Gratzel, M. J. *J. Phys. Chem.* **1991**, *95*, 877-886.

(29) Strong, L.; Whitesides, G. M. *Langmuir* **1988**, *4*, 546-558.

(30) Bain, C. D.; Whitesides, G. M. *J. Am. Chem. Soc.* **1989**, *111*, 7164-7175.

(31) Bain, C. D.; Evall, J.; Whitesides, G. M. *J. Am. Chem. Soc.* **1989**, *111*, 7155-7164.

(32) Li, Y.-Q.; Chailapakul, O.; Crooks, R. M. *J. Vac. Sci. Technol.* **1995**, *B13*, 1300-1306.

(33) Schoer, J. K. *Interface* **1995**, *4*, 56-57.

(34) Crooks, R. M.; Chailapakul, O.; Ross, C. B.; Sun, L.; Schoer, J. K. In *Interfacial Design and Chemical Sensing*; T. E. Mallouk and D. J. Harrison, Eds.; American Chemical Society: Washington, D.C., 1994; Vol. 561; pp 104-122.

(35) Wilbur, J. L.; Kumar, A.; Kim, A.; Whitesides, G. M. *Adv. Mater.* **1994**, *6*, 600.

(36) López, G. P.; Biebuyck, H. A.; Harter, R.; Kumar, A.; Whitesides, G. M. *J. Am. Chem. Soc.* **1993**, *115*, 10774-10781.

(37) López, G. P.; Biebuyck, H. A.; Whitesides, G. M. *Langmuir* **1993**, *9*, 1513-1516.

(38) Kumar, A.; Whitesides, G. M. *Appl. Phys. Lett.* **1993**, *63*, 2002-2004.

(39) Kumar, A.; Whitesides, G. M. *Science* **1994**, *263*, 60-62.

(40) Kumar, A.; Biebuyck, H. A.; Whitesides, G. M. *Langmuir* **1994**, *10*, 1498-1511.

(41) López, G. P.; Biebuyck, H. A.; Frisbie, C. D.; Whitesides, G. M. *Science* **1993**, *260*, 647-649.

(42) Kumar, A.; Biebuyck, H. A.; Abbott, N. L.; Whitesides, G. M. *J. Am. Chem. Soc.* **1992**, *114*, 9188-9189.

(43) López, G. P.; Albers, M. W.; Schreiber, S. L.; Carroll, R.; Peralta, E.; Whitesides, G. M. *J. Am. Chem. Soc.* **1993**, *115*, 5877-5878.

(44) Abbott, N. L.; Folkers, J. P.; Whitesides, G. M. *Science* **1992**, *257*, 1380.

(45) Abbott, N. L.; Whitesides, G. M.; Racz, L. M.; Szekely, J. *J. Am. Chem. Soc.* **1994**, *116*, 290-294.

(46) Abbott, N. L.; Kumar, A.; Whitesides, G. M. *Chem. Mater.* **1994**, *6*, 596-602.

(47) Abbott, N. L.; Rolison, D. R.; Whitesides, G. M. *Langmuir* **1994**, *10*, 2672.

(48) Lercel, M. J.; Rooks, M.; Tiberio, R. C.; Craighead, H. G.; Sheen, C. W.; Parikh, A. N.; Allara, D. L. *J. Vac. Sci. Technol. B.* **1995**, *13*, 1139.

(49) Gillen, G.; Wright, S.; Bennett, J.; Tarlov, M. J. *Appl. Phys. Lett.* **1994**, *65*, 534.

(50) Chan, K. C.; Kim, T.; Schoer, J. K.; Crooks, R. M. *J. Am. Chem. Soc.* **1995**, *117*, 5875-5876.

(51) Dressick, W. J.; Calvert, J. M. *Jpn. J. Appl. Phys.* **1993**, *32*, 5829.

(52) Li, Y.; Huang, J.; McIver, R. T. J.; Hemminger, J. C. *J. Am. Chem. Soc.* **1992**, *114*, 2428-2432.

(53) Huang, J.; Hemminger, J. C. *J. Am. Chem. Soc.* **1993**, *115*, 3342-3343.

(54) Huang, J.; Dahlgren, D. A.; Hemminger, J. C. *Langmuir* **1994**, *10*, 626-628.

(55) Tarlov, M. J.; Newman, J. G. *Langmuir* **1992**, *8*, 1398-1405.

(56) Tarlov, M. J.; Burgess, D. R. F., Jr.; Gillen, G. *J. Am. Chem. Soc.* **1993**, *115*, 5305-5306.

(57) Wollman, E. W.; Frisbie, C. D.; Wrighton, M. S. *Langmuir* **1993**, *9*, 1517-1520.

(58) Wollman, E. W.; Kang, D.; Frisbie, C. D.; Lorkovic, I. M.; Wrighton, M. S. *J. Am. Chem. Soc.* **1994**, *116*, 4395-4404.

(59) Graham, R. L.; Bain, C. D.; Biebuyck, H. A.; Laibinis, P. E.; Whitesides, G. M. *J. Phys. Chem.* **1993**, *97*, 9456-9464.

(60) Laibinis, P. E.; Graham, R. L.; Biebuyck, H. A.; Whitesides, G. M. *Science* **1991**, *254*, 981-983.

(61) Marrian, C. R. K.; Perkins, F. K.; Brandow, S. L.; Koloski, T. S.; Dobisz, E. A.; Calvert, J. M. *Appl. Phys. Lett.* **1994**, *64*, 390.

(62) Corbitt, T. S.; Crooks, R. M.; Ross, C. B.; Hampden-Smith, M. J.; Schoer, J. K. *Adv. Mater.* **1993**, *5*, 935-938.

(63) Kim, Y.-T.; Bard, A. J. *Langmuir* **1992**, *8*, 1096-1102.

(64) Kim, Y.-T.; McCarley, R. L.; Bard, A. J. *Langmuir* **1993**, *9*, 1941-1944.

(65) Edinger, K.; Gölzhäuser, A.; Demota, G. K.; Wöll, C.; Grunze, M. *Langmuir* **1993**, *9*, 4-8.

(66) Demir, U.; Balasubramanian, K. K.; Cammarata, V.; Shannon, C. *J. Vac. Sci. Technol., B* **1995**, *13*, 1294-9.

(67) Stroscio, J. A.; Eigler, D. M. *Science* **1991**, *254*, 1319-1326 and references therein.

(68) Staufer, U. In *Scanning Tunneling Microscopy II*; R. Wiesendanger and H.-J. Güntherodt, Eds.; Springer-Verlag: New York, 1992; Vol. 28; pp 273-302 and references therein.

(69) Parkinson, B. In *Supramolecular Architecture: Synthetic Control in Thin Films and Solids*; T. Bein, Ed.; ACS: Washington, D.C., 1992; Vol. 499; pp 76-85 and references therein.

(70) Quate, C. F. *Springer Ser. Solid State Sci.* **1992**, *111 (Low Dimensional Electronic Systems)*, 85-96 and references therein.

(71) *Scanning Tunneling Microscopy and Spectroscopy: Theory, Techniques and Applications*; Bonnell, D. A., Ed.; VCH: New York, 1993, pp 1-436 and references therein.

(72) *Scanning Tunneling Microscopy*; Stroscio, J. A.; Kaiser, W. J., Eds.; Academic Press: London, 1993; Vol. 27, pp 1-459 and references therein.

(73) McCarley, R. L.; Dunaway, D. J.; Willicut, R. J. *Langmuir* **1993**, *9*, 2775-2777.

(74) Poirier, G. E.; Tarlov, M. J. *Langmuir* **1994**, *10*, 2853-2856.

(75) Poirier, G. E.; Tarlov, M. J. *J. Phys. Chem.* **1995**, *99*, 10960-10964.

(76) Poirier, G. E.; Tarlov, M. J.; Rushmeier, H. E. *Langmuir* **1994**, *10*, 3383-3386.

(77) Sprik, M.; Delamarche, E.; Michel, B.; Röthlisberger, U.; Klein, M. L.; Wolf, H.; Ringsdorf, H. *Langmuir* **1994**, *10*, 4116-4130.

(78) Delamarche, E.; Michel, B.; Gerber, C.; Anselmatti, D.; Güntherodt, H.-J.; Wolf, H.; Ringsdorf, H. *Langmuir* **1994**, *10*, 2869.

(79) Sellers, H.; Ulman, A.; Shnidman, Y.; Eilers, J. E. *J. Am. Chem. Soc.* **1993**, *115*, 9389.

(80) Thomas, R. C.; Houston, J. E.; Crooks, R. M.; Kim, T.; Michalske, T. A. *J. Am. Chem. Soc.* **1995**, *117*, 3830-3834.

(81) Thomas, R. C. Ph. D. Dissertation, The University of New Mexico, 1994.

(82) Bartell, L. S.; Betts, J. F. *J. Phys. Chem.* **1960**, *64*, 1075-1076.

(83) Bewig, K. W.; Zisman, W. A. *J. Phys. Chem.* **1963**, *67*, 130-135.

(84) Levine, O.; Zisman, W. A. *J. Phys. Chem.* **1957**, *61*, 1188-1196.

(85) Schneider, T. W.; Buttrey, D. A. *J. Am. Chem. Soc.* **1993**, *115*, 12391-12397.

(86) Sun, L.; Crooks, R. M. *J. Electrochem. Soc.* **1991**, *138*, L23-L25.

(87) Snyder, S. R. *J. Electrochem. Soc.* **1992**, *139*, 5C.

(88) Hsu, T. *Ultramicroscopy* **1983**, *11*, 167-172.

(89) Hsu, T.; Cowley, J. M. *Ultramicroscopy* **1983**, *11*, 239-250.

(90) Schmidt, L. D. *CRC Critical Rev. Solid State Mater. Sci.* **1978**, *7*, 129-141.

(91) Gwathmey, A. T.; Cunningham, R. E. *Adv. Catal.* **1958**, *10*, 57-95.

(92) Sun, L.; Crooks, R. M. *Langmuir* **1993**, *9*, 1951-1954.

(93) Schoer, J. K.; Ross, C. B.; Sun, L.; Crooks, R. M., Unpublished results.

(94) In a previous publication (Ref 3) we indicated that scanning the surface with these mild conditions could lead to rapid modification of the surface. The sample from which we obtained the data in Figure 1 of reference 3 had been exposed to Cu underpotential deposition (UPD) and cyclic voltammetry prior to scanning by STM. As a result, the SAM had been disrupted before the STM images were obtained. Interestingly, this method may have future utility for facilitating the patterning.

(95) We define the RMS Roughness Factor (RRF) as RRF = (RMS Roughness of patterned area)/(RMS Roughness of the unpatterned terrace)

(96) Schönenberger, C.; Sondag-Huethorst, J. A. M.; Jorritsma, J.; Fokkink, L. G. J. *Langmuir* **1994**, *10*, 611-614.

(97) Bucher, J.-P.; Santesson, L.; Kern, K. *Langmuir* **1994**, *10*, 979-983.

(98) We also occasionally observe this type of behavior after patterning large features (≥ 500 nm x 500 nm) with biases ≤ ~3.5 V, when patterning the surface in low humidity environments, and we frequently observe this behavior when working in solution (Ref 99).

(99) Schoer, J. K.; Ross, C. B.; Sun, L.; Zamborini, F. P., Li, Y., Chailapakul, O., Crooks, R. M., Unpublished results.

(100) Delamarche, E.; Michel, B.; Kang, H.; Gerber, C. *Langmuir* **1994**, *10*, 4103-4108.

(101) Because patterned areas become roughened compared to the unpatterned surface, individual depth profiles become difficult to interpret meaningfully. To minimize this problem, we obtained average depth profiles through the patterns. An average depth profile is the average of numerous parallel depth profiles. This procedure effectively reduces the contribution of features with extreme dimensions.

(102) *Scanning Tunneling Microscopy II*; Wiesendanger, R.; Güntherodt, H.-J., Eds.; Springer-Verlag: Heidelberg, 1992; Vol. 28, pp 1-308 and references therein.

(103) *Scanning Tunneling Microscopy and its Applications*; Bai, C., Ed.; Springer-Verlag: Heidelberg, 1992; Vol. 32, pp 1-331 and references therein.

(104) Chen, C. J. *Introduction to Scanning Tunneling Microscopy*; Oxford University Press: New York, 1993, pp 1-412 and references therein.

(105) These types of changes in the imaging ability of the tip can frequently be eliminated by pulsing the bias to +3 - +4 V for <1 s. These brief pulses generally result in the formation of a mound(s) on the surface, suggesting that material is transferred from the tip to the surface.

(106) We typically observe less than 2 nm of drift during 4 patterning scans at 41 Hz scan rate and 256 x 256 pixel resolution (about 25 s).

(107) Zamborini, F. P.; Schoer, J. K.; Crooks, R. M., Unpublished results.

(108) To minimize the extent of surface contamination, we prepared the Au ball, mounted it, briefly cleaned it in an Ar plasma, and then immediately imaged and patterned it. All imaging and patterning were completed within 65 min of plasma cleaning. We did not observe significant formation of Au oxide from the plasma cleaning when we electrochemically analyzed such a surface. However, we did observe a slight increase in the RMS roughness of the surface after plasma cleaning.

(109) It can be challenging to obtain reliable measurements of surface features on nominally naked Au in air because the patterns begin to fill in and change shape immediately after fabrication. As shown in Figure 6, there are no such surface mobility problems with ODM-coated Au surfaces. However, we have observed that short-chain *n*-alkyl mercaptans facilitate Au surface mobility.

Table I. Physical characteristics of the pattern shown in Figure 4 as a function of the number of patterning scans (standard patterning conditions).

Number of Patterning Scans	Unpatterned Terrace	Primary Pattern			Secondary Pattern		
	RMS Roughness (nm)	RMS Roughness (nm)	RMS Roughness Factor[84]	Depth (nm)	RMS Roughness (nm)	RMS Roughness Factor[84]	Depth (nm)
Pre-pattern	0.08	0.08	1.0	0.00	0.07	0.9	0.00
1	0.07	0.16	2.3	0.32	0.10	1.4	0.10
10	0.06	0.11	1.7	0.30	0.10	1.6	0.11
60	0.07	0.12	1.7	0.62	0.11	1.6	0.13
250	0.10	0.75	7.7	3.09	0.15	1.7	0.22

Table II. Physical characteristics of the pattern shown in Figure 6 as a function of time.

Pattern Description	Unpatterned Terrace RMS Roughness (nm)	Pattern RMS Roughness (nm)	RMS Roughness Factor^{95}	Pattern Depth (nm)
Pre-pattern	0.09	0.09	1.0	0.00
Post-pattern	0.09	0.26	2.9	0.50
Post-pattern + 24 h	0.09	0.23	2.6	0.51
Post-pattern + 48 h	0.09	0.23	2.6	0.48
Post-pattern + 71 h	0.09	0.23	2.5	0.49
Post-pattern + 95 h	0.10	0.23	2.3	0.49

Figure Captions

Figure 1. A series of STM images illustrating the types of tip-induced modification that can occur on an ODM-coated Au(111) surface after imaging for prolonged time periods using standard imaging conditions (SIC) or scanning across a highly terraced region with high tip velocity. (a) STM image of an ODM surface prior to repeated imaging. (b) STM image obtained after scanning the central 500 nm x 500 nm area 4 times with SIC, except a more rapid scan rate of 41 Hz was used to accelerate tip-induced modification. (c) STM image of the region enclosed by the dashed box in (b) obtained immediately after frame (b). (d) STM image of the same region shown in (c) after scanning the same area with SIC for more than 3.5 h. The gray scale is 2 nm in all images.

Figure 2. (a) STM image of a nominally 1 μm x 1 μm pattern within an ODM SAM confined to a Au(111) surface. Conditions for the patterning were 4 patterning scans at +8.0 V bias, 2 Hz scan rate, 150 pA tunneling current, and 256 x 256 pixel resolution. The pattern was then swept 4 times with SIC, except the scan rate was reduced to 2 Hz, to remove loosely bound debris. The gray scale is 4 nm. (b) Average depth profile centered on the horizontal line through the pattern in (a). (c) STM image of a nominally 50 nm x 50 nm pattern fabricated using SPC and 4 scans. The gray scale is 2 nm. (d) Average depth profile centered on the vertical line through the pattern in (c).

Figure 3. STM images of an ODM-coated Au(111) surface obtained: (a) before, (b) after, and (c)-(f) sequentially during fabrication of a nominally 100 nm x 100 nm pattern with 4 scans using SPC. The gray-scale is 2 nm in each image.

Figure 4. Results of repetitively patterning a nominally 50 nm x 50 nm feature into an ODM-coated Au(111) surface using SPC. The images were obtained after: (a) 1, (b) 10, (c) 60, and (d) 250 patterning scans. The images are inverted and displayed in three dimensions to emphasize the pattern dimensions. Table I lists some physical characteristics of the pattern. (e) Plot of the pattern depth as the number of patterning scans is increased. The inset shows the results of the first 28 patterning scans. (f) Plot of the RRF as a function of the number of patterning scans. The inset shows the results of the first 40 patterning scans.

Figure 5. Results of repetitively sweeping a nominally 100 nm x 100 nm feature in an ODM-coated Au(111) surface using SIC. The pattern was fabricated with 4 scans using SPC. The images were obtained: (a) immediately after fabrication and (b) after scanning the patterned area 8 times with SIC. The images are inverted and displayed in three dimensions to emphasize the change in the depth of the pattern. The gray-scale is 2 nm in each image. (c) Plot of the net pattern depth versus the number of sweep scans. (d) Plot of the RRF as a function of the number of sweep scans.

Figure 6. (a) STM image of an ODM-coated Au(111) surface obtained immediately after fabricating a nominally 50 nm x 50 nm pattern with 4 scans using SPC. (b) STM image of the same feature after the scanning was disabled and the tip was parked more than 2 μm away from the pattern for 24 h. The gray-scale is 2 nm in each image. Table II lists some physical characteristics of the pattern at intervals covering 5 days.

Figure 7. (a) STM image of an unpatterned, naked Au(111) surface. b) STM image of the area shown in (a) after fabricating a nominally 50 nm x 50 nm pattern with 4 scans using SPC. The images are inverted and displayed in three dimensions to emphasize the pattern dimensions.

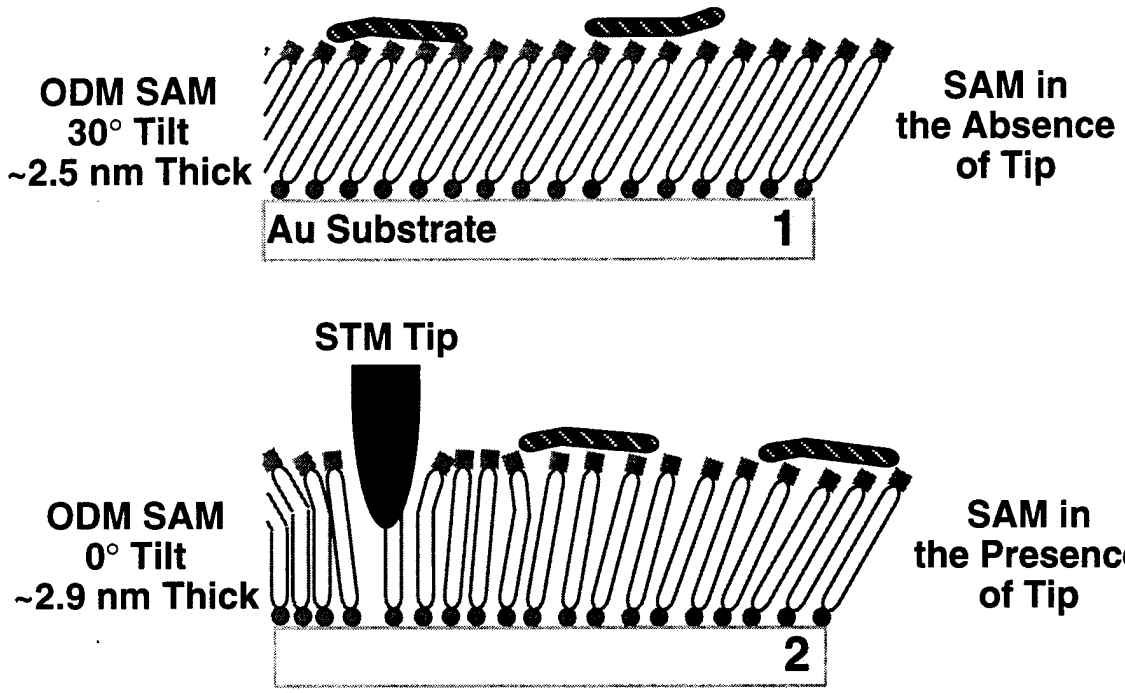

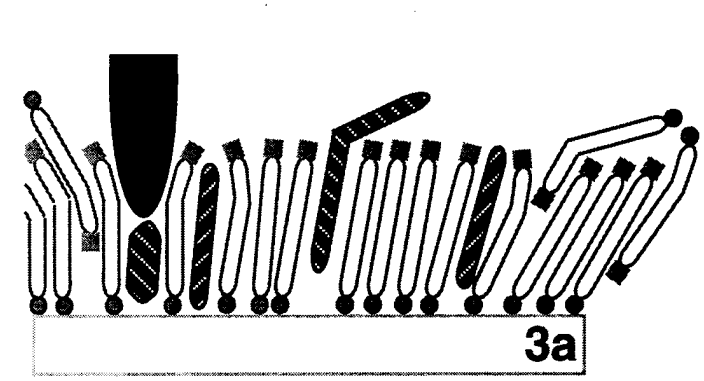

Standard Imaging Conditions (SIC)
(Mechanical)

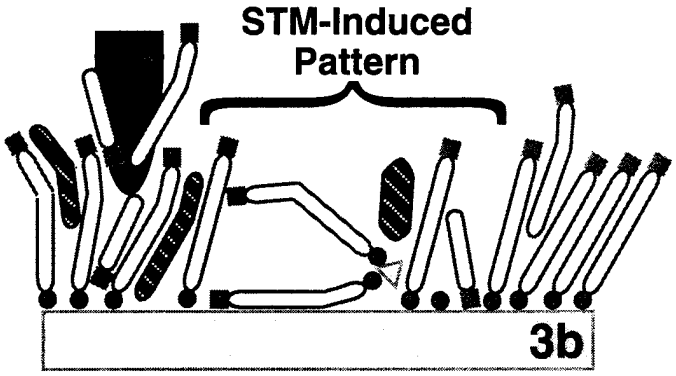

Standard Patterning Conditions (SPM)
(Electrochemical/Mechanical)

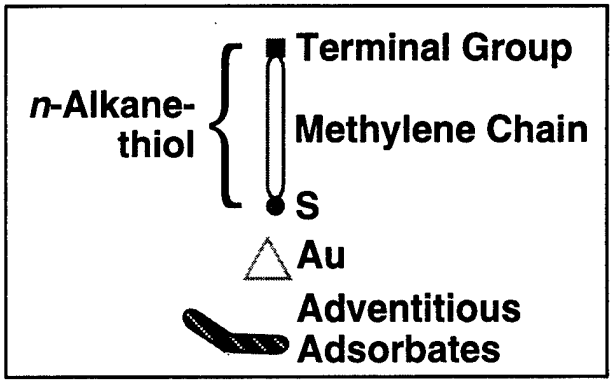

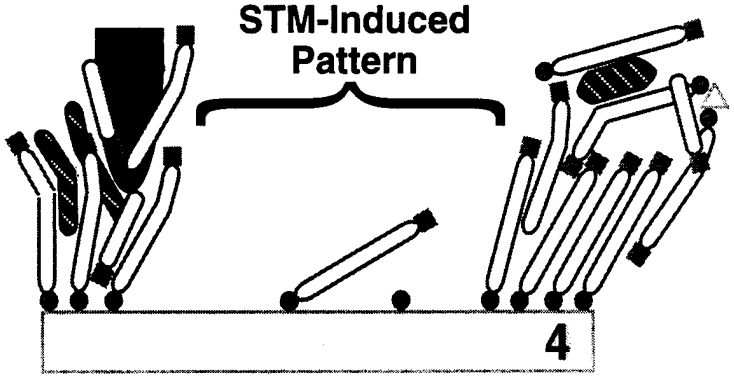

Sweeping
(mechanical)

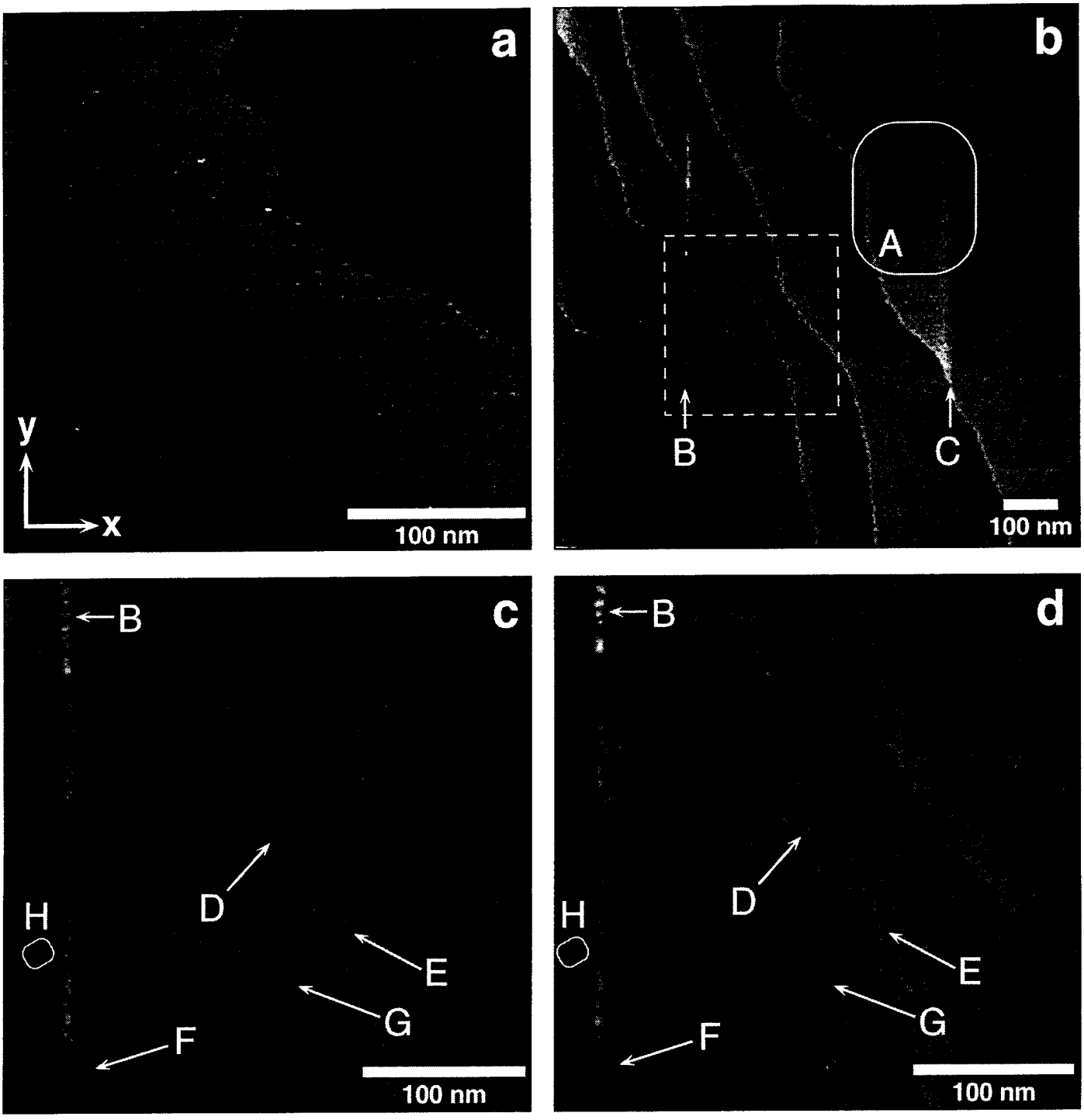

Schoer & Crooks/Figure 1

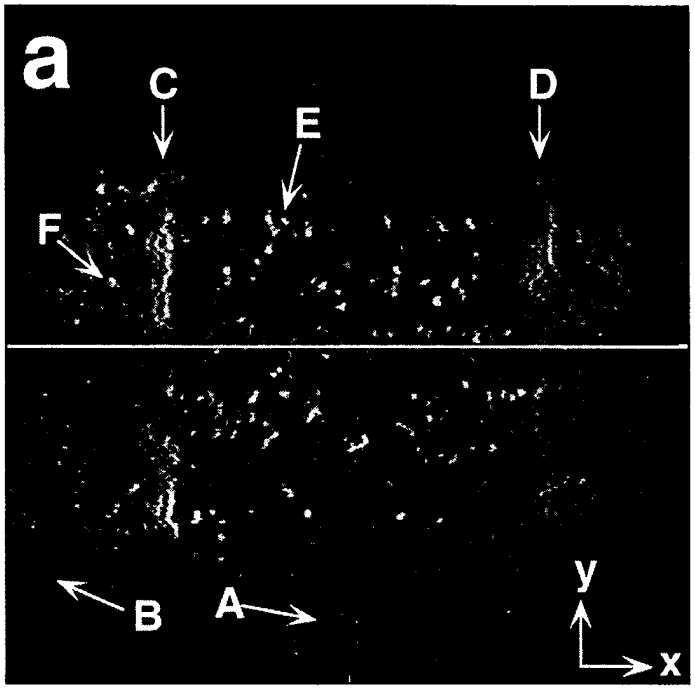

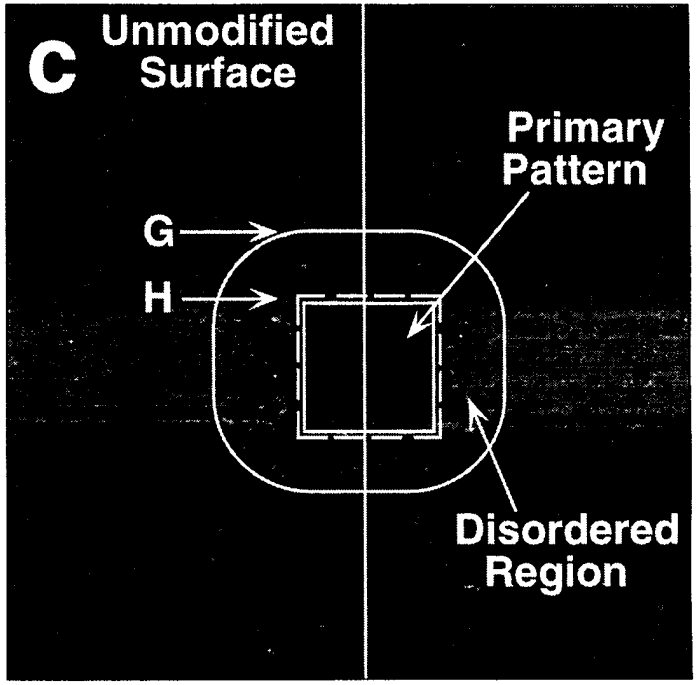

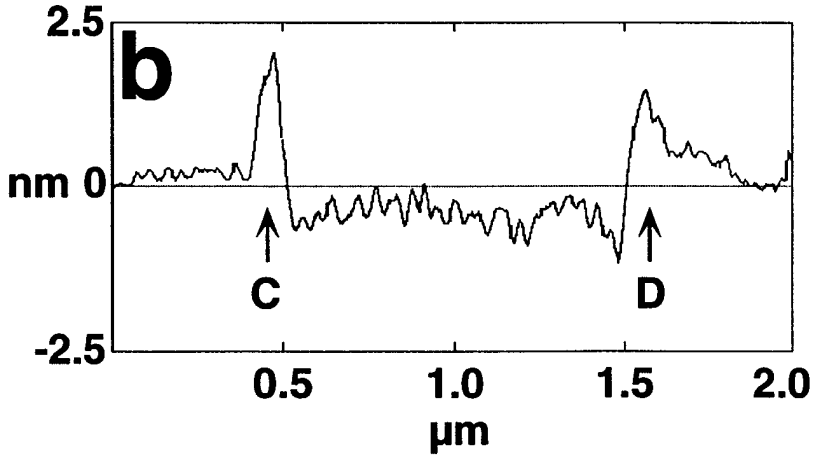

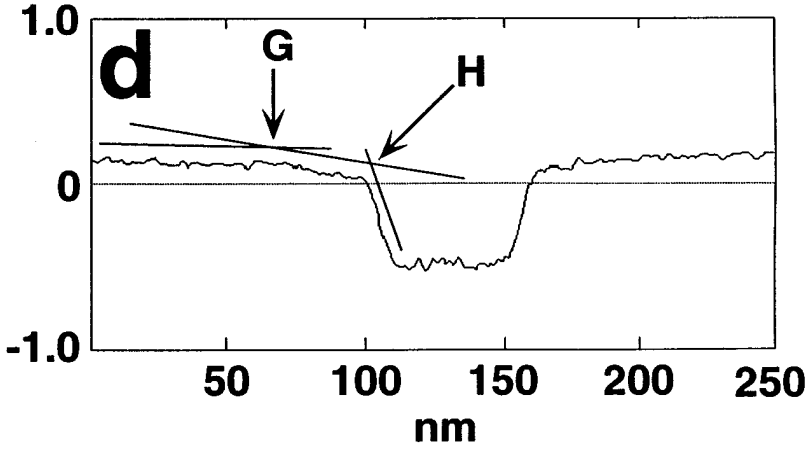

Schoer & Crooks/Figure 2

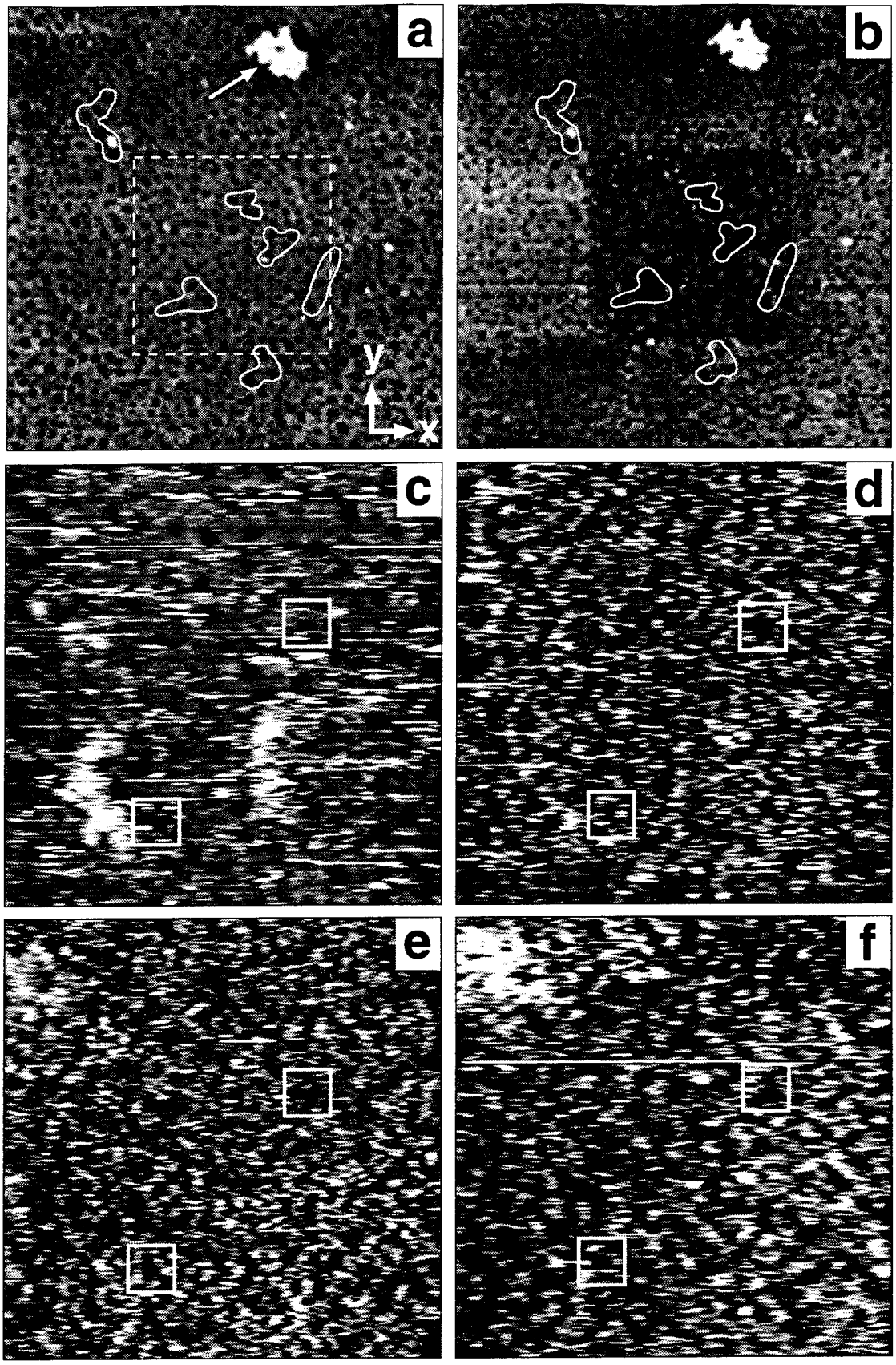

Schoer & Crooks/Figure 3

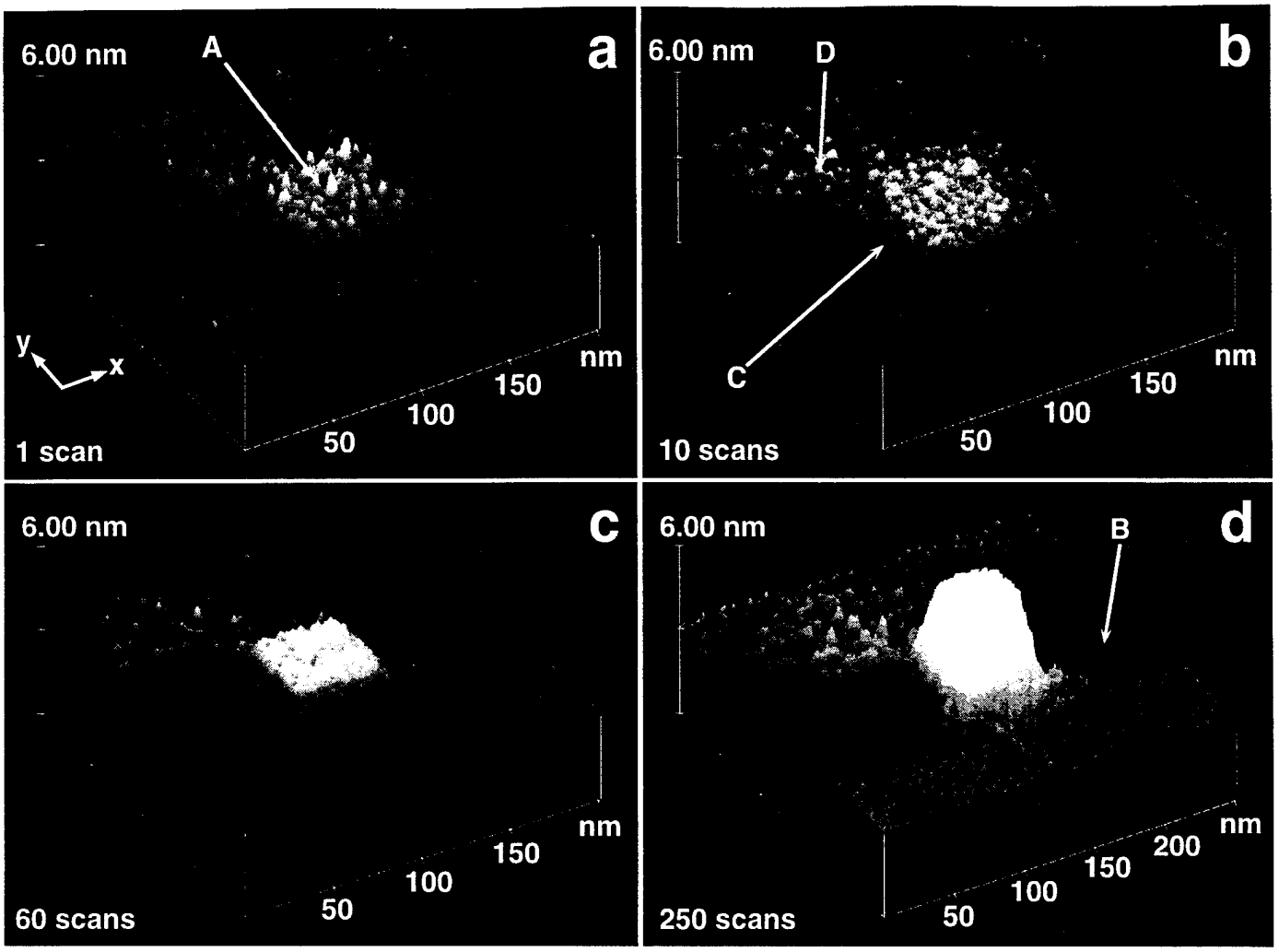

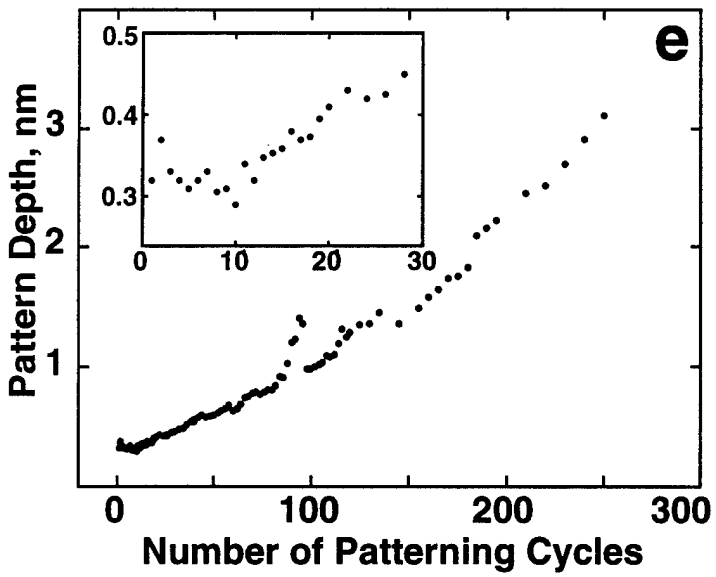

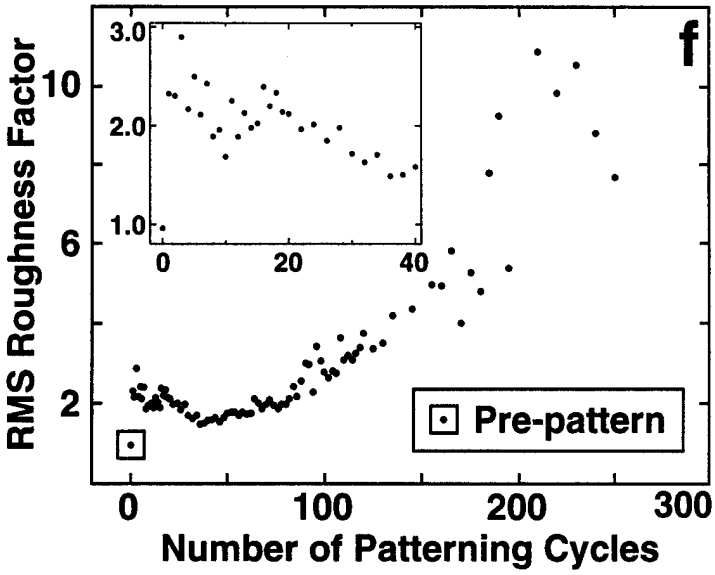

Schoer & Crooks/Figure 4

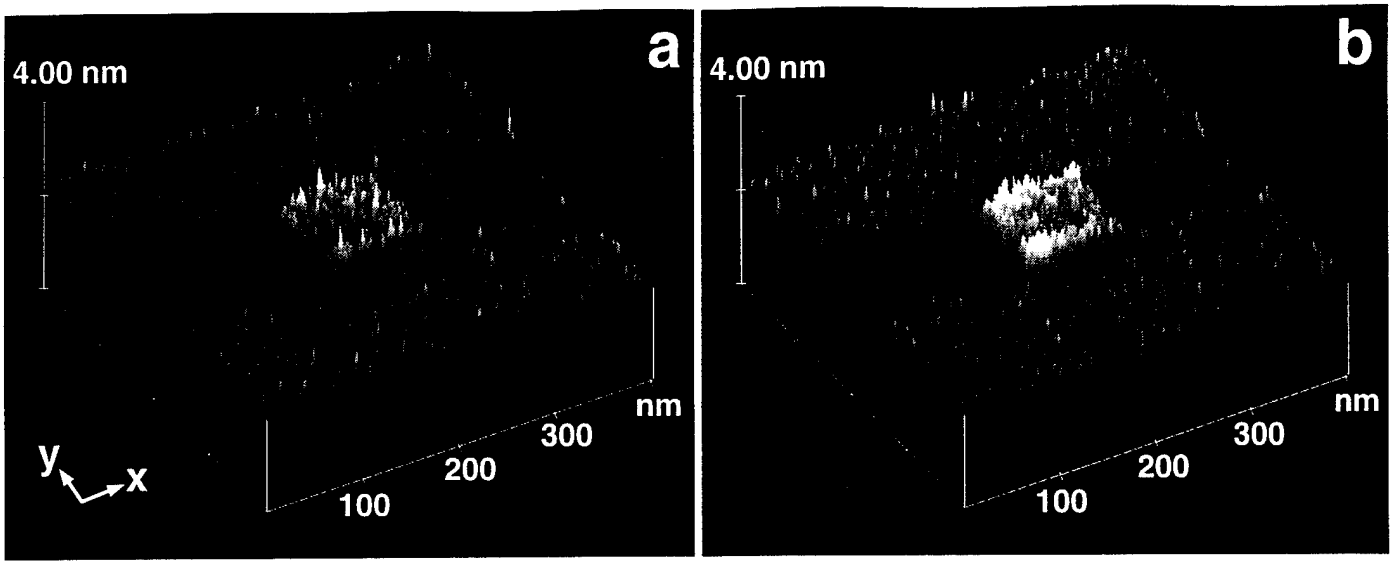

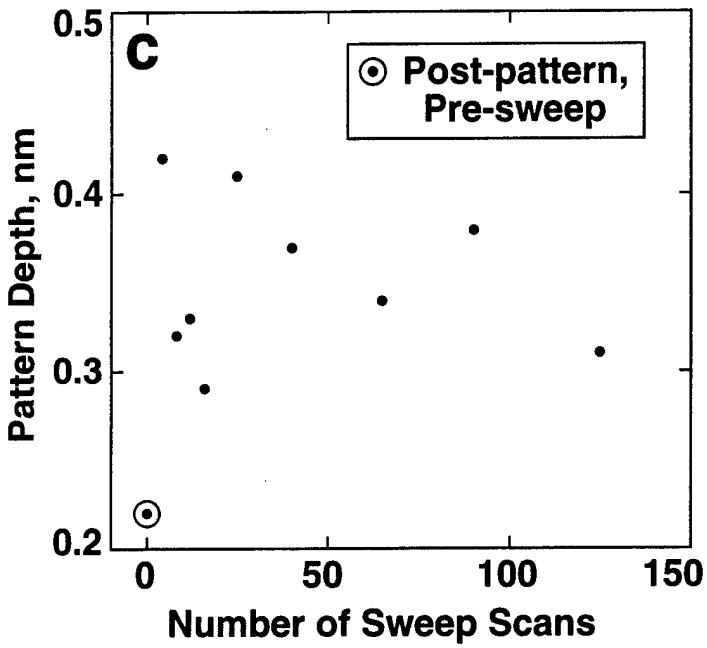

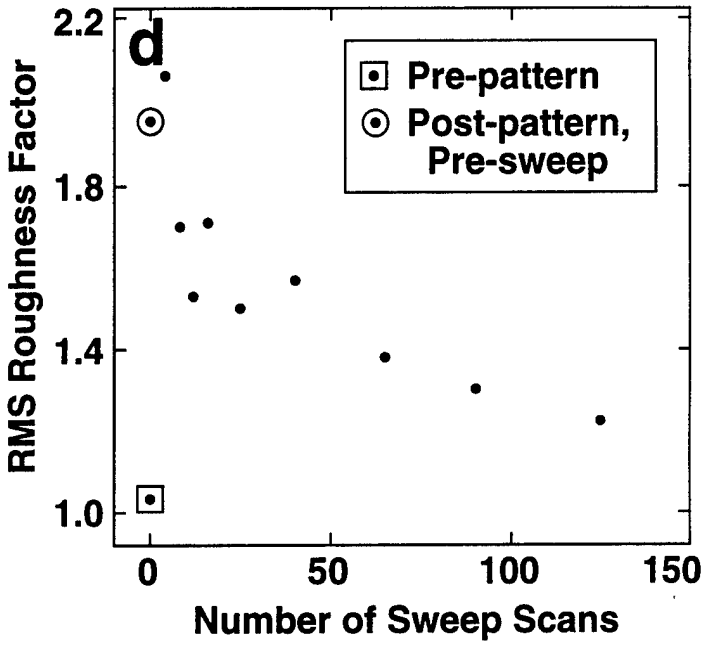

Schoer & Crooks/Figure 5

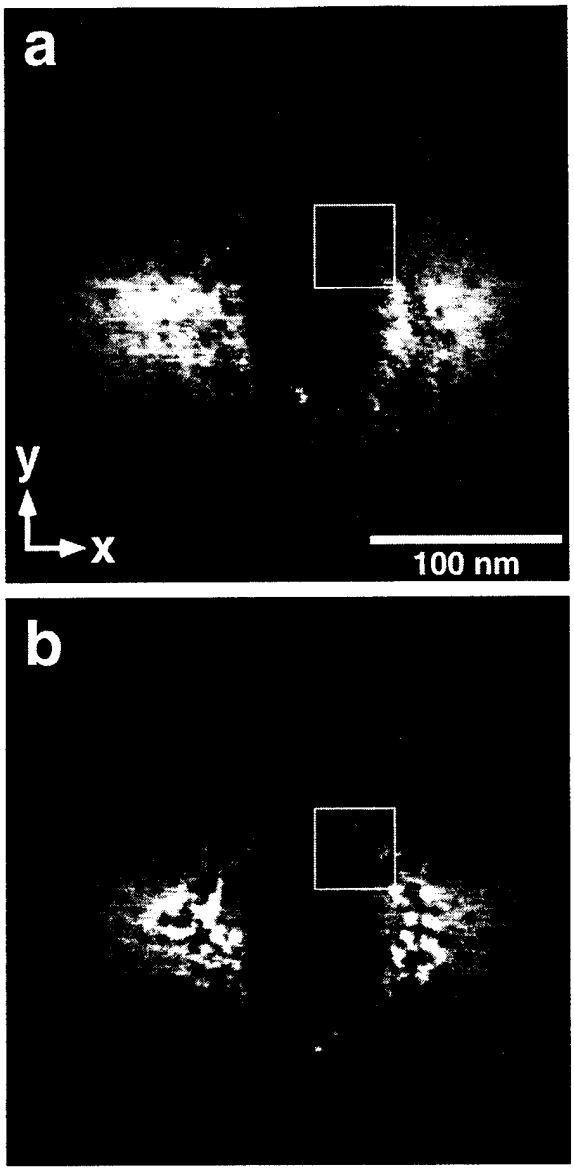

Schoer & Crooks/Figure 6

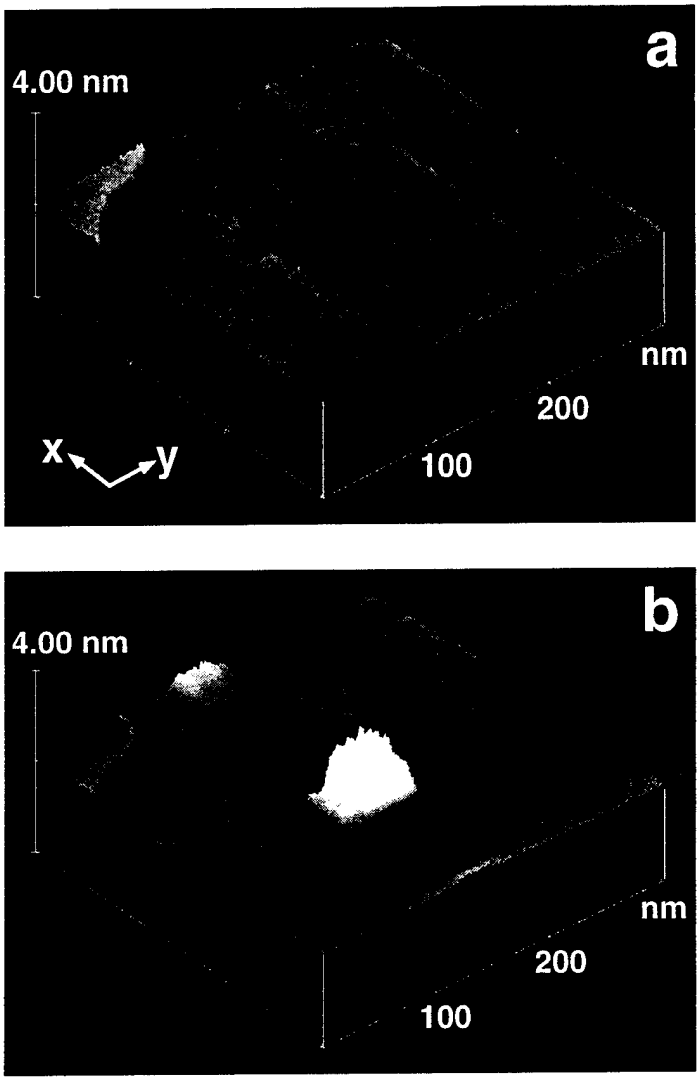

Schoer & Crooks/Figure 7